Massive Star Formation: The Power of Interferometry

Henrik Beuther

Max Planck Institute for Astronomy
Königstuhl 17, 69117 Heidelberg, Germany
beuther@mpia.de

Abstract

This article presents recent work to constrain the physical and chemical properties in high-mass star formation based largely on interferometric high-spatial-resolution continuum and spectral line studies at (sub)mm wavelengths. After outlining the concepts, potential observational tests, a proposed evolutionary sequence and different possible definitions for massive protostars, four particular topics are highlighted: (a) What are the physical conditions at the onset of massive star formation? (b) What are the characteristics of potential massive accretion disks and what do they tell us about massive star formation in general? (c) How do massive clumps fragment, and what does it imply to high-mass star formation? (d) What do we learn from imaging spectral line surveys with respect to the chemistry itself as well as for utilizing molecules as tools for astrophysical investigations?

1 Introduction

Star formation is a key process in the universe, shaping the structure of entire galaxies and determining the route to planet formation. In particular, the formation of massive stars impacts the dynamical, thermal and chemical structure of the interstellar medium (ISM), and it is almost the only mode of star formation observable in extragalactic systems. During their early formation, massive star-forming regions inject energy to the ISM via their outflows and jets, then during their main sequence evolution, the intense uv-radiation of the massive stars heats up their environment, and at the very end of their life, Supernovae stir up the ISM by their strong explosions. Furthermore, massive stars are the cradles of the heavy elements. Hence, life as we know it today would not exist if massive stars had not formed first the heavy elements in their interiors via nucleosynthesis. In addition to this, almost all stars form in clusters, and within the clusters massive stars dominate the overall luminosities. Isolated low-mass star formation is the exception, and isolated high-mass star formation likely does not exist

Concepts: In spite of their importance, many physical processes during the formation of massive stars are not well understood. While there exists a paradigm for low-mass star formation on which large parts of the scientific community agree (e.g., Andre et al. 2000; McKee & Ostriker 2007),

this is less the case for high-mass star formation (e.g., Beuther et al. 2007a; Zinnecker & Yorke 2007). The conceptional problem is based on the fact that at least in spherical symmetry the radiation pressure of a centrally ignited star $\geq 8\,M_\odot$ would be large enough to stop any further gas infall and hence inhibit the formation of more massive objects. Over the last decade, two schools have been followed to solve this problem: (a) The turbulent accretion scenario, which is largely an enhancement of the low-mass star formation scenario, forms massive stars in a turbulent core with high accretion rates and a geometry including accretion disks and molecular outflows (e.g., Yorke & Sonnhalter 2002; McKee & Tan 2003; Krumholz et al. 2007b; Keto 2007). In contrast to that, (b) the competitive accretion scenario relies on the clustered mode of massive star formation. In this scenario, the accretion rates are determined by the whole cluster potential, and those sources sitting closest to the potential well will competitively accrete most of the mass (e.g., Bonnell et al. 2004, 2007).

Potential observational tests: How can we observationally discriminate between the different scenarios? For example, the turbulent accretion scenario predicts qualitatively similar outflow and disk properties as known for low-mass stars, however, with quantitatively enhanced parameters like the accretion rates, outflow energies, or disk sizes. In contrast to that, modeling of the proto-cluster evolution in the competitive accretion scenario indicates extremely dynamic movements of all cluster-members throughout their whole evolution. It is unlikely that in such a dynamic environment collimated outflows or large disks could survive at all. Another difference between both scenarios is based on their early fragmentation predictions. While the turbulent accretion scenario draws their initial gas clumps from (gravo-)turbulently fragmented clouds (e.g., Padoan & Nordlund 2002) and these gas clumps do not fragment afterwards much anymore, the competitive accretion scenario predicts that the initial gas clumps fragment down to many clumps all of the order a Jeans-mass ($\sim 0.5\,M_\odot$). Hence, while in the former scenario, the Initial Mass Function (IMF) is determined during the early cloud fragmentation processes, the latter models predict that the IMF only develops during the ongoing cluster formation. Therefore, studying the initial fragmentation and the early core mass functions can give insights in the actual massive star formation processes.

Evolutionary sequence: Independent of the formation scenario, there has to be an evolutionary sequence in which the processes take place. For this review, I will follow the evolutionary sequence outlined by Beuther et al. (2007a): Massive star-forming regions start as High-Mass Starless Cores (HMSCs), i.e., these are massive gas cores of the order a few 100 to a few $1000\,M_\odot$ without any embedded protostars yet. In the next stage we have High-Mass cores with embedded low- to intermediate-mass protostars below $8\,M_\odot$, which have not started hydrogen burning yet. During that evolutionary phase, their luminosity should still be dominated by accretion luminosity. Following that, the so called High-Mass Protostellar Objects (HMPOs) are still massive gas cores but now they contain embedded massive protostars $>8\,M_\odot$ that have started

hydrogen burning which soon dominates the total luminosity of the sources. Hot Molecular Cores (HMCs) and hypercompact HII regions (HCHIIs) are part of that class. The last evolutionary stage then contains the final stars that have stopped accreting. While most ultracompact HII regions (UCHIIs) are likely part of the latter group, some of them may still be in the accretion phase and could then hence still harbor HMPOs.

Definitions of a massive protostar: Another debate in massive star formation centers around the exact definition of a "massive protostar". If one followed the low-mass definition which basically means that a protostars is an object that derives most of its luminosity from accretion, then "massive protostars" should not exist or only during a very short period of time because as soon as they are termed "massive" ($>8\,M_{\odot}$), their luminosity is quickly dominated by hydrogen burning. In this scenario, during the ongoing formation processes, one would then need to talk about "accreting stars". This approach is for example outlined by Zinnecker & Yorke (2007). A different definition for "massive protostars" is advocated, e.g., recently by Beuther et al. (2007a): In this picture, a protostar is defined in the sense that each massive object that is still in its accretion phase is called a "massive protostar", independent of the dominating source of luminosity. This definition follows more closely the usual terminology of "proto", meaning objects that are not finished yet.

Observational challenges: Whatever physical or chemical processes we are interested in massive star formation, one faces severe observational challenges because of the clustered mode of massive star formation and the on average large distances of a few kiloparsec. Therefore, high spatial resolution is a prerequisite for any such study. Furthermore, the early stages of massive star formation are characterized by on average cold gas and dust temperatures which are best observed at (sub)mm wavelength. Hence, most observations presented in the following are based on (sub)mm interferometer observations of young massive star-forming regions at different evolutionary stages.

The main body of this article is divided into four sections dealing first with the initial conditions that are present prior to or at the onset of massive star formation. The next two sections deal with our current knowledge about the properties of potential massive accretion disks and the fragmentation behavior of massive gas clumps and cores. The following section will then outline the status and future possibilities of astrochemical investigations. Finally, I try to sketch the directions where current and future answers to the questions raised in the Abstract may lead to.

2 The earliest stages of massive star formation

What are the initial conditions of massive star formation? Until a few years ago, to address this question observationally in a statistical sense was close to impossible because we had no means to identify large samples of sources prior to or at the onset of massive star formation. The situation has changed significantly since the advent of the space-based near- and mid-infrared missions

that surveyed the Galactic plane starting with ISO and MSX, and now conducted with much better sensitivity and spatial resolution by Spitzer. These missions have revealed more than 10^4 Infrared Dark Clouds (IRDCs), which are cold molecular clouds that are identified as shadows against the Galactic background (e.g., Egan et al. 1998; Carey et al. 2000; Simon et al. 2006). These clouds are characterized by on average cold temperatures ($\sim$15 K), large masses (a few 100 to a few 1000 $M_\odot$) and average densities of the order $10^4 - 10^5\,cm^{-1}$ (e.g., Rathborne et al. 2005; Sridharan et al. 2005; Pillai et al. 2006a). Although these clouds appear as dark shadows, they may be starless but they can also harbor embedded forming protostars. In fact, a statistical analysis of the percentage of starless IRDCs versus IRDCs with embedded protostars will be an important step to understand the time-scales important for the earliest evolutionary stages. Currently, the statistical database of in depth IRDC studies is still insufficient for such an estimate (e.g., Rathborne et al. 2005, 2006; Pillai et al. 2006b; Beuther & Steinacker 2007; Motte et al. 2007), however, it is interesting to note that until now no starless IRDC has been unambiguously identified in the literature, all detailed studies revealed embedded star formation processes. To first order, this triggers the interpretation/speculation that the high-mass starless core phase is likely to be extremely shortlived. Future investigations of larger samples will answer this question more thoroughly.

Figure 1: Sample IRDCs from Sridharan et al. (2005): MSX A-band (8 μm) images (black is bright) with 1.2 mm emission contours: The first two numbers refer to the corresponding IRAS source and the third number labels the mm sub-sources. The five-pointed stars mark cores lacking good 1.2 mm measurements.

In a recent spectral line study of a sample of 43 IRDCs (Fig. 1), Beuther & Sridharan (2007) detected SiO(2–1) emission from 18 sources. Assuming that SiO is produced solely through sputtering from dust grains, and that this sample is representative for IRDCs in general, it indicates that at least 40% of the IRDCs have ongoing outflow activity. Since the non-detection of SiO does not imply no outflow activity, this number is a lower limit, and even a higher percentage of sources may harbor already ongoing star formation. The range of observed SiO line-widths down to zero intensity varied between 2.2 and 65 $km\,s^{-1}$. While inclination effects and embedded objects of different mass could account for some of the differences, such effects are unlikely causing the whole velocity spread. Therefore, Beuther & Sridharan (2007) speculate whether the varying SiO line-widths are also indicators of their evolutionary stage with the smallest line-width close after the onset of star formation activity. In the same study, Beuther & Sridharan (2007) observed CH_3OH and CH_3CN. While CH_3CN was detected only toward six sources, CH_3OH was found in approximately 40% of the sample. The derived column densities are low of the order 10^{-10} with respect to H_2. These values are consistent with chemical models of the earliest evolutionary stages of high-mass star for-

mation (e.g., Nomura & Millar 2004), and the CH_3OH abundances compare well to recently reported values for low-mass starless cores (e.g., Tafalla et al. 2006).

Zooming into selected regions in more detail, we studied one particularly interesting IRDC at high angular resolution with the Plateau de Bure Interferometer and the Spitzer Space Telescope (IRDC 18223-3, see Fig. 1 right panel; Beuther et al. 2005a; Beuther & Steinacker 2007). Combining the Spitzer mid-infrared data between 3 and 8 μm with the 3.2 mm long-wavelengths observations from the Plateau de Bure Interferometer (PdBI), we did not find any mid-infrared counterpart to the massive gas core detected at 3.2 mm (Fig. 2, Beuther et al. 2005a). However, we did detect three faint 4.5 μm features at the edge of the central 3.2 mm continuum core. Since emission features that occur only in the 4.5 μm but no other Spitzer band are usually attributed to shocked H_2 emission from molecular outflows (e.g., Noriega-Crespo et al. 2004), we concluded that the region likely hosts a very young protostar that drives a molecular outflow but that is still too deeply embedded by to be detected by the Spitzer IRAC bands. This interpretation found further support by line-wing emission in older CO and CS data. Based on the inferred central source, we predicted that the region should have a strongly rising spectral energy distribution (SED) and hence be detected at longer wavelengths. As soon as the MIPSGAL mid- to far-infrared survey with Spitzer became available, we then could identify the central source at 24 and 70 μm (Fig. 2, Beuther & Steinacker 2007). Combing the available mid-/far-infrared data with the long-wavelengths observations in the mm regime, it is possible to fit the SED with a two component model: one cold component ($\sim$15 K and $\sim$576 $M_\odot$) that contains most of the mass and luminosity, and one warmer component ($\sim$51 K and $\sim$0.01 $M_\odot$) to explain the 24 μm data. The integrated luminosity of $\sim$177 $L_\odot$ can be used to constrain additional parameters of the embedded protostar from the turbulent core accretion model for massive star formation (McKee & Tan 2003). Following the simulations by Krumholz et al. (2007b), the data of IRDC 18223-3 are consistent with a massive gas core harboring a low-mass protostellar seed of still less than half a solar mass with high accretion rates of the order $10^{-4}\,M_\odot yr^{-1}$ and an age below 1000 yrs. In the framework of this model, the embedded protostar is destined to become a massive star at the end of its formation processes. While this interpretation is attractive, it is not unambiguous, and especially the derived time-scale from this model appears short when comparing with recent outflow data that will be presented in the following section (§3.1).

In summary, these observations indicate that the physical and chemical conditions at the onset of low- and high-mass star formation do not differ significantly (except for largely different initial cloud clump masses and accretion rates), and that the time-scale for massive bound gas clumps to remain starless is likely relatively short.

Figure 2: IRDC 18223-3 images at different wavelengths from Beuther & Steinacker (2007). The color scales show Spitzer images at various wavelength, and the contours show the 93 GHz (3.2mm) continuum emission observed with the PdBI (Beuther et al. 2005a). The left panel presents a three-color composite with blue 3.6 μm, green 4.5 μm and red 8.0 μm (adapted from Beuther et al. 2005a). The inlay zooms into the central core region. The middle and right panel show the Spitzer 24 and 70 μm images, respectively. The circles in each panel present the Spitzer beam sizes and the ellipse in the left panel presents the PdBI 3.2 mm continuum synthesized beam. A size-ruler is also shown in the left panel.

3 Massive accretion disks?

As mentioned in the Introduction, molecular outflows and accretion disks can be used to discriminate between the different formation scenarios for massive stars. Massive outflows have been subject to intense studies for more than a decade (e.g., Shepherd & Churchwell 1996; Beuther et al. 2002b; Zhang et al. 2005; Arce et al. 2007), and although there is considerable discussion about the details, we find a growing consensus that massive molecular outflows are ubiquitous in high-mass star formation, and that collimated jet-like outflows do exist for massive sources as well, at least during the very early evolutionary stages (Beuther & Shepherd 2005). The collimation of the outflows is likely to widen with ongoing evolution. Nevertheless, these data are consistent with the turbulent core model for massive star formation, whereas they are less easy to reconcile with the competitive accretion model because the latter is so dynamic that collimated structures likely could not survive very long. Furthermore, the existence of collimated outflows can only be explained by magneto-hydrodynamic acceleration of the jet from an underlying accretion disk. Hence, there is ample indirect evidence for massive accretion disks, however, the physical characterization of disks in massive star formation is still lacking largely the observational basis (Cesaroni et al. 2007). The two main reasons for this are that the expected massive accretion disks are still deeply embedded within their natal cores complicating the differentiation of the disk emission from the ambient core, and that the clustered mode of massive star formation combined with the large average distances of the targets makes spatially resolving structures of the order 1000 AU a difficult observational task. In spite of these difficulties, the advent of broad spectral bandpasses allowing us to study several spectral lines simultaneously, as well as the improved spatial resolution of existing and forthcoming interferometers have increased the number of disk studies over the last few years. For a recent review see Cesaroni et al. (2007).

Here, I will show three different examples of disk and/or rotation candidates in an evolutionary sense: It starts with a rotation and outflow investigation of the previously discussed IRDC 18223-3 (§2), then I will present recent data from the high-mass disk candidate in the HMPO IRAS 18089-1732, and finally observations from a massive disk candidate at a more evolved evolu-

tionary stage will be discussed.

3.1 Rotation in IRDCs: the case of IRDC 18223-3

As a follow-up of the Infrared Dark Cloud study of IRDC 18233-3 discussed in §2, Fallscheer et al. (in prep.) observed the same region with the Submillimeter Array (SMA) in several spectral setups around 230 and 280 GHz covering outflow as well as dense gas tracers. Figure 3 shows a compilation of the CO(2–1) data, one CH_3OH line and the dust continuum emission. The blue- and red-shifted CO(2–1) emission clearly identifies at least one large-scale outflow in the north-west south-east direction. This is consistent with two of the 4.5 μm emission features at the edge of the core (Fig. 2, left panel and inlay). There is another collimated red-shifted feature to the south-west corresponding to the third 4.5 μm feature, however, we do not identify a blue counterpart and refrain from further interpretation of that feature. Since we find for the main north-west south-east outflow blue- and red-shifted emission on both sides of the continuum peak, the orientation of the outflow should be close to the plane of the sky (see, e.g., models by Cabrit & Bertout 1990), and hence the assumed underlying perpendicular rotating structure close to edge-on. Following the approach outlined in Beuther et al. (2002b), the outflow mass and outflow rate are 13 $M_\odot$ and $3.5 \times 10^{-4}\,M_\odot yr^{-1}$, respectively. With the above derived core mass of $\sim$576 $M_\odot$ (§2), this source fits well into the correlation between outflow rate and core mass previously derived for HMPOs (Fig. 7 in Beuther et al. 2002b).

Figure 3: SMA observations toward IRDC 18223-3 (Fallscheer et al. in prep.). The left panel shows the blue- and red-shifted CO(2–1) emission as solid and dashed contours overlaid on the grey-scale 1.3 mm dust continuum emission. The central core is the same source as in Fig. 2. The right panel presents in grey-scale a 1st moment map (intensity weighted velocity distribution) of CH_3OH overlaid with the 1.1 mm continuum emission. The empty and full circle are the synthesized beams of the line and continuum emission, respectively.

While the outflow rate is consistent with the accretion rate previously derived from the SED (§2), discrepancies arise with respect to the age of the system. Although dynamical timescales are highly uncertain (e.g., Parker et al. 1991), the size of the molecular outflow combined with a low inclination angle allows for at least a timescale estimate for the outflow of the order a few 10^4 yrs, well in excess of the value $\leq 10^3$ yrs previously derived from the SED applied to models (§2). Notwithstanding the large errors between the different estimates, the discrepancy of more than an order of magnitude appears real. How can we explain that? There is no clear answer to that yet, but a possibility is that the orientation of the disk-outflow system with the disk close to edge-on absorbs a large amount of flux distorting the SED on the Wien-side. If that were the case, the SED-estimated age could underestimate the age of the system. Another possibility to solve the discrepancy is that

the initial start of high-mass star formation may proceed slower, i.e., the first low-mass protostar(s) (destined to become massive or not?) form within the massive cores, and they already start driving outflows, but at that stage it is impossible to detect them in the near- to far-infrared because of the large extinction. In this picture at some point the high-mass star formation process would need to accelerate because otherwise the massive stars cannot form in the short time-scales of a few 10^5 yrs (e.g., McKee & Tan 2002). It is not clear why the whole process should start slow and what could trigger such acceleration later-on. Obviously, more theoretical and observational work is required to explain the different time-scales in more detail.

Figure 3 (right panel) zooms into the central core and shows dust continuum emission as well as the velocity structure of the dense central gas observed in $CH_3OH(6_{0,1} - 5_{0,1})$ with a lower level excitation level of $E_{\rm low} = 34.8\,{\rm K}$. Interestingly, both the continuum and the spectral line emission are elongated in the north-east south-west direction perpendicular to the main molecular outflow. While the continuum emission shows three resolved emission features, CH_3OH exhibits a smooth velocity gradient across the source spanning approximately $3\,{\rm km\,s^{-1}}$. The CH_3OH line-width FWHM toward the continuum peak is $2.1\,{\rm km\,s^{-1}}$. The blue-redshifted features in the north-west are likely part of the molecular outflow and one sees even a slight elongation of the continuum emission in that direction. While CH_3OH is a well-known shock tracer and hence regularly found within molecular outflows (e.g., Bachiller et al. 2001), it is more of a surprise that we find it in an elongated structure likely associated with rotation and infall perpendicular to the outflow. The extent of this structure is large with $\sim$6.5″ corresponding to more than 20000 AU at the given distance of 3.7 kpc. Although we have no methanol isotopologue in the setup to exactly determine the opacity of the line, a low-energy transition like this is likely to be optically thick. Hence, we are tracing some of the outer rotating structures, probably corresponding to a larger scale rotating and potentially infalling/inspiralling toroid (e.g., Cesaroni et al. 2005; Keto 2007). The small velocity spread across the structure as well as the relatively narrow CH_3OH line-width toward the core center are also consistent with tracing outer structures because due to momentum conservation rotating structures should have lower velocities further out.

Notwithstanding that we do not exactly know the age of IRDC 18223-3, its non-detection up to $8\,\mu$m puts it at an early evolutionary phase prior to the better studied HMPOs and Hot Molecular Cores. Our data clearly show that even at such early stages molecular outflows and rotating structures perpendicular to that have been developed, and it is likely that closer toward the core center, one will find a real accretion disk. To investigate the latter in more detail, higher angular resolution observations of an optically thin dense gas tracer are required.

3.2 The HMPO disk candidate IRAS 18089-1732

As a more evolved massive disk candidate, we have studied intensely over the last few years the HMPO IRAS 18089-1732. This source at a distance of 3.6 kpc with a luminosity of $10^{4.5}\,L_{\odot}$ is part of a large sample of HMPOs, it hosts H_2O and Class II CH_3OH maser and has strong molecular line emission indicative of en embedded Hot Molecular Core (Sridharan et al. 2002; Beuther et al. 2002a). During early SMA observations Beuther et al. (2004c,a, 2005c) identified in SiO a molecular outflow in the north-south direction, and perpendicular to that in $HCOOCH_3$ a velocity gradient on scales of a few 1000 AU. Although these data were indicative of rotation and an underlying massive accretion disk, the observations did not allow us to characterize the structure in more detail because of a lack of spatial resolution. Therefore, we observed IRAS 18089-1732 now in high-energy transitions of NH_3 at 1.2 cm wavelength with the VLA and the ATCA at a spatial resolution of 0.4″ (Beuther & Walsh 2008). These NH_3(4,4) and (5,5) lines have a two-fold advantage: Their high excitation levels (> 200 K) ensure that we are tracing the warm inner regions and are less confused by the surrounding cold envelope, whereas the cm wavelengths regime is less affected by high optical depth of the dust emission in high column density regions and may hence be particularly well suited for massive disk studies (e.g. Krumholz et al. 2007a). Figure 4 presents an integrated image and a 1st moment map (intensity weighted velocity) of the corresponding VLA observations.

Figure 4: The left panel shows the VLA NH_3(5,5) emission integrated from 31 to 37 km s^{-1} (Beuther & Walsh 2008). The right panel presents the corresponding 1st moment map contoured from 31.5 to 36.5 km s^{-1} (step 1 km s^{-1}). The white-black dashed contours show the 1.2 cm continuum emission. The asterisks mark the position of the submm continuum peak (Beuther et al. 2005c), and the synthesized beams are shown at the bottom-left (grey NH_3 and dashed 1.2 cm emission).

The 1st moment map confirms the previously assessed velocity gradient in east-west direction perpendicular to the molecular outflow. The NH_3 linewidth FWHM toward the central core is 4.7 km s^{-1}, significantly broader than that of IRDC 18223-3 (§3.1). In the simple picture of equilibrium between gravitational and centrifugal force, the rotationally bound mass would be $\sim$37 $M_{\odot}$, of the same order as the whole gas mass as well as the mass of the central source (of the order 15 $M_{\odot}$). Furthermore, the position-velocity diagram is not consistent with Keplerian rotation. It even shows indications of super-Keplerian motion, which is expected for very massive disks where the rotation profile is not only determined by the mass of the central object but also by the disk itself (e.g., Krumholz et al. 2007b). Hence, the new VLA and ATCA data clearly confirm the previous assessment of rotation perpendicular to the outflow/jet, however, the kinematic signatures of that rotating structure are not consistent with a Keplerian disk like in low-mass

star formation, but they show additional features which can be produced by massive self-gravitating disks as well as by infalling gas that may settle eventually on the disk. In addition to this, the detection of the high-excitation lines in the rotating material indicates high average gas temperatures >100 K for the disk-like structures, well in excess of typical gas temperatures in low-mass disks of the order 30 K (e.g., Piétu et al. 2007). Moreover, we detect double-lobe cm continuum emission close to the core center where the two lobes are oriented in north-south direction parallel to the outflow identified in SiO. With respect to previous data at longer wavelength, we find a spectral index at cm wavelength of 1.9, consistent with an optically thick jet (Reynolds 1986).

It will be interesting to further zoom into the innermost regions with future instruments like ALMA and eVLA to asses whether the quantitative deviations from typical low-mass accretion disks continue down to the smallest scales, or whether we will find Keplerian disk structures as known from their low-mass counterparts.

3.3 A more evolved massive disk candidate?

Moving along in the evolutionary sequence, we have recently identified a potential disk around a more evolved candidate young stellar object (Quanz et al. in prep.). The source labeled so far mdc1 (massive disk candidate) was identified serendipitously during a near-infrared wide-field imaging campaign on Calar Alto via its K-band cone-like nebulosity and a central dark lane (Fig. 5). First single-dish bolometer and spectral line measurements revealed a 1.2 mm flux of 12 mJy and a velocity of rest of $\sim$51 km s^{-1}. The latter value indicates a kinematic distance of $\sim$5 kpc, consistent with distances of a few UCHII regions in the surrounding neighborhood. To investigate this object in more detail, we recently observed it with the SMA at 1.3 mm wavelength mainly in the mm continuum and the ^{12}CO/C^{18}O spectral line emission. Figure 5 presents an overlay of the SMA data with the K-band nebulosity, and a few points need to be stressed:

Figure 5: The grey-scale in both panels shows the K-band near-infrared nebulosity observed for this massive evolved disk candidate (Quanz et al. in prep.). The contours are the corresponding SMA mm observations where the left panel shows the 1.3 mm continuum emission, and the right panel in black and white contours the blue-shifted ^{12}CO(2–1) and the integrated C^{18}O(2–1) emission, respectively.

(a) Although spatially unresolved with a synthesized beam of $\sim 4.0''$ the 1.3 mm continuum peak exactly coincides with the infrared dark lane consistent with the large column densities of the proposed disk-like structure. The flux measured with the SMA is 12 mJy like the previous single-dish measurements. This indicates that we have no surrounding dust/gas envelope but rather an isolated central structure. Assuming optically thin dust emission

at 50 K, the approximate gas mass of the central structure is $\sim$5 $M_\odot$. (b) We detect blue-shifted CO(2–1) spatially well correlated with the K-band nebulosity north of the dark lane. This confirms the initial interpretation of that feature to be due to an outflow. (c) The integrated $C^{18}O$(2–1) emission is elongated perpendicular to the outflow observed in CO and K-band continuum emission. The line-width FWHM of the $C^{18}O$ emission is narrow with $\sim$0.8 km s^{-1}, however, the spatial extent of this structure is large, of the order 2×10^4 AU.

While the low gas mass and the missing more massive gas envelope could be interpreted in the framework of a low-mass source, such large disk-structures as indicated by the $C^{18}O$ emission are not known from typical low-mass disk sources (e.g., Simon et al. 2000). Therefore, these observations can also be interpreted as a remnant disk/torus around an intermediate to high-mass (proto)star that has already dispersed much of its envelope. Although $C^{18}O$ is detected only in two channels, these show a clear velocity shift, and the small line-width may be due to the lower rotational motions on large scales assuming momentum conservation in rotating, potentially Keplerian structures.

Synthesizing the three example sources shown here, it is interesting to note that the line-widths are small in the youngest and the supposed to be oldest source, whereas they are large in the HMPO which should be in its main accretion phase. In an evolutionary picture this can be interpreted that at early evolutionary stages infall, turbulence and rotation are not yet that vigorous. Then in the main accretion phase, infall, rotation and outflow processes strongly increase the line-width. And finally, when the accretion stops, the envelope and disk slowly disperse and one observes only a remnant structure with small line-width in the outer regions. This scenario is speculative, however, the number of disk candidates is steadily increasing, and since we start sampling more evolutionary stages, we are getting the chance to address disk evolution questions in high-mass star formation as well.

4 Fragmentation in high-mass star formation

How massive gas clumps fragment is one of the key questions if one wants to understand the formation of the Initial Mass Function, and as outlined in §1, the two main massive star formation theories predict differences in the early fragmentation processes. In the following I will present several examples of fragmenting massive cores addressing issues about fragmentation on the cluster-scale, fragmentation of smaller groups, potential proto-trapezia, and the determination of density structures of sub-sources within evolving clusters.

4.1 Resolving the massive proto-cluster IRAS 19410+2336

To address fragmentation processes at early evolutionary stages high angular resolution at (sub)mm wavelengths is the tool of choice to resolve the relevant substructures. Beuther & Schilke (2004) resolved the young massive star-forming region IRAS 19410+2336 (distance $\sim$2.1 kpc and luminosity $\sim 10^4\,L_\odot$) at 1.3 mm wavelength with the PdBI at approximately 2000 AU linear resolution into 24 sub-sources. Although from a statistical point of view such numbers cannot compete with the clusters exceeding 100 or even 1000 stars observed at optical and near-infrared wavelength, this is still one of the prime examples of a spatially resolved massive proto-cluster. Assuming that all emission features are due to cold dust emission from embedded protostars, they were able to derive a core-mass function. With a power-law slope of -2.5, this core mass function is consistent with the Salpeter IMF slope of -2.35 (Salpeter 1955). Therefore, Beuther & Schilke (2004) interpreted these observations as support for the turbulent fragmentation put forth by, e.g., Padoan & Nordlund (2002).

A few caveats need to be kept in mind: While Beuther & Schilke (2004) assumed a uniform gas temperature for all sub-sources, it is more likely that the central peaks are warmer than those further outside. This issue can be addressed by spectral line emission with temperature sensitive molecules (e.g., H_2CO) which is an ongoing project by Rodon et al. (in prep.). Furthermore, the assumption that all mm continuum peaks are of pro- or pre-stellar nature is not necessarily always valid, e.g., Gueth et al. (2003) or Beuther et al. (2004b) have shown that mm continuum emission can partly also be caused by collimated jets. However, only the central source is detected at cm wavelength and collimated jets should be detectable at cm wavelengths as well. Therefore, we believe that jets should not affect the analysis much.

Independent of the caveats, it is surprising that IRAS 19410+2336 is still the only young massive star-forming region that is resolved in >10 sub-sources in the mm continuum emission. While this can be explained to some degree by the exceptionally good uv-coverage obtained for the given observations, which results in a good sampling of spatial structures, we also need to consider whether different modes of fragmentation may exist. Similar high-spatial-resolution studies of more proto-clusters spanning a broad range of luminosities are required to tackle this question in more detail. Another interesting question is associated with the spatial filtering of interferometers and the corresponding large-scale emission: Many interferometric (sub)mm continuum studies of massive star-forming regions filter out of the order 90% of the flux, hence, large amounts of the gas are distributed on larger scales, usually $> 10''$. The question remains whether this gas will eventually participate in the star formation process or not?

4.2 Fragmentation of potential proto-trapezia

4.2.1 The enigmatic proto-trapezium W3-IRS5

The W3-IRS5 region is one of the prototypical high-mass star-forming regions with $\sim 10^5\,L_\odot$ at a distance of $\sim$1.8 kpc that shows fragmentation on scales of the order 1000 AU observed at near-infrared as well as cm wavelengths (Megeath et al. 2005; van der Tak et al. 2005). However, not much was known about the cold dust and gas emission. Therefore, we observed the region with the PdBI at 1.3 and 3.5 mm wavelengths with the new extended baselines resulting in an unprecedented spatial resolution of $\sim 0.37''$ (Rodon et al. in prep.). Figure 6 shows a compilation of the 1.3 mm continuum data and the SiO(5–4) and $SO_2(22_{2,20} - -22_{1,21})$ spectral line emission.

Figure 6: PdBI observations of the W3-IRS5 system from Rodon et al. (in prep.). The left panel shows the 1.3 mm continuum emission, and the stars mark near-infrared sources from Megeath et al. (2005). The middle panel presents as solid and dotted contours the blue- and red-shifted SiO(5–4) emission overlaid on the grey-scale 1.3 mm continuum emission. The right panel finally shows the 1st moment map of $SO_2(22_{2,20} - -22_{1,21}$ in grey-scale with the 1.3 mm continuum contours.

The mm continuum emission resolves the W3-IRS5 region into five sub-sources, where four of them are coincident with near-infrared and cm emission peaks. Three of the sources are clustered in a very small projected volume of only $\sim$2000 AU. With this high spatial resolution we find extremely large average column densities of the order a few times $10^{24}\,cm^{-2}$ which corresponds to visual extinctions A_v between 5×10^3 and 10^4 averaged over the beam size. Such extinctions should be far too large to allow any detection at near-infrared wavelengths, nevertheless, near-infrared counterparts are detected (Megeath et al. 2005). This conundrum can likely be explained by the detection of several SiO outflows in the field. In particular, we find very compact blue- and red-shifted SiO emission toward the two main mm peaks, where the blue- and red-shifted emission is barely spatially separated (Fig. 6 middle panel). Since the overall time-scale of the W3-IRS5 outflow system is relatively large (of the order a few times 10^4 yrs, Ridge & Moore 2001), these compact features are unlikely from very young outflows, but they indicate that the outflows are oriented almost along the line of sight. The opening cones of the outflows are the likely cause that emission from close to the protostars can escape the region and hence make them detectable at near-infrared wavelengths.

The right panel of Fig. 6 shows the 1st moment map of SO_2 (intensity weighted velocities) which encompasses the mm continuum peaks. The coherent velocity field over the sub-sources is a strong indicator that the system is a bound structure and not some unbound chance alignment within the field (e.g., Launhardt 2004). In addition to the general velocity gradient from the south-east to the north-west, one tentatively identifies velocity gradients across the two strongest mm continuum peaks. Since we do not know the

exact orientation of the outflows with respect to the SO_2 rotation axis, it is not yet possible to identify these structures with disk-like components as in §3. Future observations in different tracers may help to shed more light on the rotational structure associated with each sub-source. It should also be noted that the line-width FWHM toward the mm continuum peaks varies between 6.2 and 7 $\mathrm{km\,s^{-1}}$ larger than those reported in §3. While the larger line-width compared with the IRDC and the more evolved source may be explained by the evolutionary sequence sketched at the end of §3, the larger FWHM compared to the HMPO may have different reasons, among them are the larger luminosity of W3-IRS5, its multiplicity compared with the so far unresolved source IRAS 18089-1732, and also the molecular species, because SO_2 should be more affected by shocks than the NH_3 line used for the IRAS 18089-1732 study. In addition to this, the SO_2 moment map exhibits a velocity discontinuity with a velocity jump of the order 4 $\mathrm{km\,s^{-1}}$ south-east of the mm continuum peaks. What is the cause of this discontinuity, is it associated with the original core formation and a shock within converging flows, or is it of different origin?

In summary, the combination of high-spatial-resolution observations of the continuum emission in addition to outflow and dense gas tracers allows us to characterize many physical properties of this proto-trapezium system with respect to its multiple components and their outflow and rotation properties.

4.2.2 Fragmentation of the hot core G29

The hot core G29.96 located right next to a well-known cometary HII region comprises another example of several protostellar submm continuum sources within the innermost center of a high-mass star forming region (distance ∼6 kpc, luminosity $9 \times 10^4\,\mathrm{L_\odot}$). High-spatial resolution observations with the SMA in its most extended configuration yielded a spatial resolution of $0.36'' \times 0.25''$ in the submm continuum at ∼348 GHz, corresponding to a linear resolution of 2000 AU (Fig. 7, Beuther et al. 2007c, the line data will be discussed in §5.1). The Hot Molecular Core previously identified in a high-excitation NH_3 line (Cesaroni et al. 1998) is resolved by these new data into four sub-sources within a projected diameter of ∼6900 AU. Assuming that the emission peaks are of protostellar nature, Beuther et al. (2007c) estimated a protostellar density of $\sim 2 \times 10^5\,\mathrm{protostars/pc^{-3}}$. This is considered a lower limit since we are limited by spatial resolution, sensitivity and projection effects. Nevertheless, such a protostellar density is about an order of magnitude higher than values usually reported for star-forming regions (e.g., Lada & Lada 2003). Although this value is still about an order of magnitude lower than protostellar densities that would be required in the merging scenario for massive stars (e.g., Bonnell et al. 2004; Bally & Zinnecker 2005), it is interesting to note that increasingly higher protostellar densities are reported when going to younger sources and better angular resolution (see also Megeath et al. 2005). This allows us to speculate whether future observations with better spatial resolution and sensitivity toward extremely massive

star-forming regions will reveal protostellar densities that may be sufficient to make mergers possible. While such a detection would not be a proof for mergers to exist, it will certainly be important to verify whether the required initial conditions do exist at all.

Figure 7: Compilation of data toward the UCHII/hot core region G29.96 from Beuther et al. 2007c. The dashed contours present the cometary UCHII regions whereas the full contours show the older NH_3 observation from the hot core (Cesaroni et al. 1994). The grey-scale with contours then present the new high-resolution ($0.36'' \times 0.25''$) submm continuum data from the SMA.

4.3 Density structure of sub-sources – IRAS 05358+3543

As a final example for the potential of (sub)mm continuum studies, I present the recent multi-wavelength investigation of the HMPO IRAS 05358+3543. This region at a distance of 1.8 kpc with a luminosity of $10^{3.8}$ $L_\odot$ was observed in a combined effort with the PdBI and the SMA at arcsecond resolution in four wavelength bands (3.1 and 1.2 mm, and 875 and 438 μm, Beuther et al. 2007b; Leurini et al. 2007). While many details about the sub-structure of the forming cluster can be derived, here, I will discuss only two results.

Based on the multi-wavelength data, Beuther et al. (2007b) fitted the spectral energy distribution on the Rayleigh-Jeans side of the spectrum (Fig. 8). While the main source can well be fitted by a typical protostellar spectrum consisting of free-free emission at long wavelength and a steep flux increase at shorter wavelength due to the dust emission, another sub-source did not fit at all into that picture. In particular the shortest wavelength data-point at 438 μm shows significantly lower fluxes than expected for a typical protostar. The most likely explanation for this effect is that we are dealing with a very cold source and that therefore we are already approaching the peak of the spectral energy distribution. The data allowed us to estimate an upper limit for the dust temperature of ≤ 20 K. Since we are also not detecting any other line emission from this core (mainly from typical hot core molecules, Leurini et al. 2007), it may well be a starless core right in the vicinity of an already more evolved massive protostar. Further investigations of this sub-source in typical cold gas tracers like N_2H^+ or NH_3 are required to test this proposal. Independent of whether this source harbors an embedded protostar or not, these observations show the importance of short wavelength data at high spatial resolution if one wants to differentiate between critical core parameters like the dust temperature.

Another physical parameter which has so far not been observationally constrained for massive star formation, is the density profile of individual sub-sources. While density profiles of low-mass star-forming cores have well been characterized (e.g., Motte et al. 1998; Ward-Thompson et al. 1999; Andre et al.

Figure 8: The left panel presents the SED toward the coldest sub-source in IRAS 05358+3543 (Beuther et al. 2007b). The parameters of the fits are marked in the figure. The right panel shows intensities averaged in uv-annuli and plotted versus the baseline-length for different sub-sources and wavelengths. Most can be well fitted by power-law distributions.

2000), in high-mass star formation, density profiles were until now only derived with single-dish observation covering scales of the whole cluster but not individual sub-sources (e.g., Beuther et al. 2002a; Mueller et al. 2002; Hatchell & van der Tak 2003). This is partly due to the technical problem of interferometer observations that filter out large amounts of the flux and hence make density profile determinations from their images extremely unreliable. To overcome this problem, Beuther et al. (2007b) analyzed the data directly in the uv-domain prior to any fourier transformation. Figure 8 shows the corresponding plots of the observed intensities versus the uv-distance for three sub-sources in three wavelengths bands, respectively. The observations cannot be fitted with Gaussian distributions, but much better fits are achieved with power-law distributions. These power-laws in the uv-domain can directly be converted to the corresponding power-laws of the intensity profiles in the image plane. Assuming furthermore a temperature distribution $T \propto r^{-0.4}$ we can now infer the density profiles of individual sub-sources of the evolving cluster. The derived density profiles $\rho \propto r^{-p}$ have power-law indices p between 1.5 and 2. Although this result is similar to the density profiles previously determined for low-mass cores, to our knowledge this is the first time that they have been observationally constrained for resolved sub-sources in a massive star-forming region. The density structure is an important input parameter for any model of star formation (e.g., McKee & Tan 2003).

5 Astrochemistry

5.1 Toward a chemical evolutionary sequence

Astrochemistry is a continuously growing field in astronomy. Although line-survey style studies of different sources have existed for quite some time (e.g., Blake et al. 1987; Schilke et al. 1997), these studies had usually been performed with single-dish instruments averaging the chemical properties over the whole cluster-forming regions. Since the advent of broadband receivers at interferometers like the SMA, it is now also possible to perform imaging spectral line surveys that allow us to spatially differentiate which molecules are present in which part of the targeted regions, for example, the spatial differentiation between nitrogen- and oxygen-bearing molecules in Orion-KL (e.g., Blake et al. 1996; Beuther et al. 2005b). In addition to the spatial analysis of individual regions, we are also interested in analyzing how the chemistry evolves in an evolutionary sense. As an early step in this direction we synthesized SMA observations that were observed in the same

spectral setup around 862 μm toward four massive star-forming regions over the last few years (Beuther et al. subm.). These four regions comprise a range of luminosities between $10^{3.8}\,L_\odot$ and $10^5\,L_\odot$, and they cover different evolutionary stages from young High-Mass Protostellar Objects (HMPOs) to typical Hot Molecular Cores (HMCs): Orion-KL: HMC, $L \sim 10^5\,L_\odot$, $D \sim 0.45$ kpc (Beuther et al. 2005b); G29.96: HMC, $L \sim 9 \times 10^4\,L_\odot$, $D \sim 6$ kpc (Beuther et al. 2007c); IRAS 23151, HMPO, $L \sim 10^5\,L_\odot$, $D \sim 5.7$ kpc (Beuther et al. 2007d); IRAS 05358: HMPO, $L \sim 10^{3.8}\,L_\odot$, $D \sim 1.8$ kpc (Beuther et al. 2007b; Leurini et al. 2007). Smoothing all datasets to the same linear spatial resolution of 5700 AU, we are now capable to start comparing these different regions. Figure 9 presents typical spectra extracted toward the HMC G29.96 and the HMPO IRAS 23151.

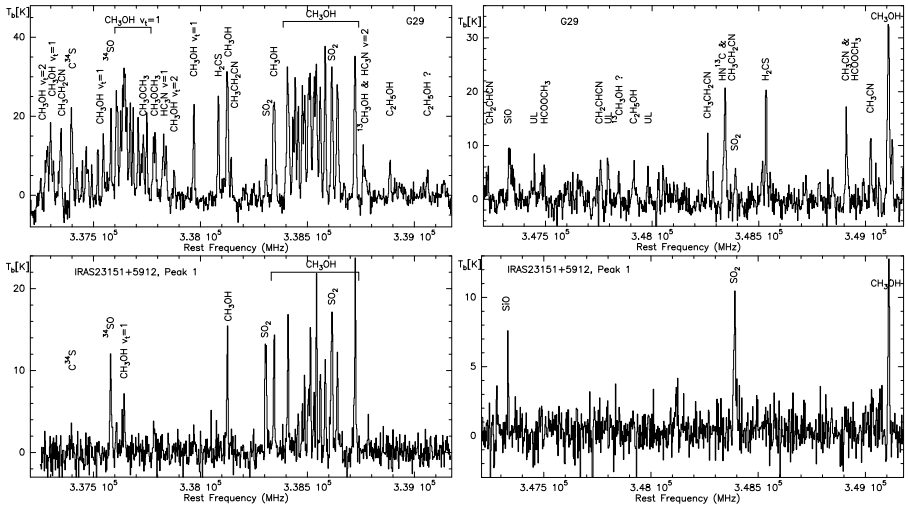

Figure 9: SMA spectra extracted toward two massive star-forming regions (G29.96 top row & IRAS 23151+5912 bottom row, Beuther et al., subm.). The spectral resolution in all spectra is 2 km/s. The left and right column show the lower and upper sideband data, respectively.

A detailed comparison between the four sources is given in a forthcoming paper (Beuther et al. subm.), here we just outline a few differences in a qualitative manner.

• The HMCs show far more molecular lines than the HMPOs. Orion-KL and G29.96 appear similar indicating that the nature of the two sources is likely to be comparable as well. Regarding the two HMPOs, the higher luminosity one (IRAS 23151) shows still more lines than the lower-luminosity source (IRAS 05358). Since IRAS 05358 is approximately three times closer to us than IRAS 23151, this is not a sensitivity issue but it is likely due to the different luminosity objects forming at the core centers.

• The ground-state CH_3OH lines are detected toward all four sources. However, the vibrational-torsional excited CH_3OH are only strongly detected to-

ward the HMCs Orion-KL and G29.96. Independent of the luminosity, the HMPOs exhibit only one CH_3OH $v_t = 1$ line, which can easily be explained by the lower average temperatures of the HMPOs.
• A more subtle difference can be discerned by comparing the SO_2 and the $HN^{13}C/CH_3CH_2CN$ line blend near 348.35 GHz (in the upper sideband). While the SO_2 line is found toward all four sources, the $HN^{13}C/CH_3CH_2CN$ line blend is strongly detected toward the HMCs, but it is not found toward the HMPOs. In the framework of warming up HMCs, this indicates that nitrogen-bearing molecules are either released from the grains only at higher temperatures, or they are daughter molecules which need some time during the warm-up phase to be produced in gas-phase chemical networks. In both cases, such molecules are not expected to be found much prior to the formation of a detectable HMC.
• Comparing the spatial distribution of different molecules, we find, e.g., that $C^{34}S$ is observed mainly at the core edges and not toward the submm continuum peak positions. This difference can be explained by temperature-selective desorption and successive gas-phase chemistry reactions: CS desorbs early from the grains at temperatures of a few 10 K and should peak during the earliest evolutionary phases toward the main continuum sources. Subsequently when the core warms up to ∼100 K, H_2O desorbs and dissociates to OH. The OH then quickly reacts with the sulphur to form SO and SO_2 which should then peak toward the main continuum sources. This is what we observe in our data. The fact that the $C^{34}S$ peaks are offset from the submm continuum condensations even toward the younger sources is due to their evolutionary stage where they have already heated up their central regions to more than 100 K. Even younger sources are required to confirm this scenario.

5.2 C_2H as a tracer of the earliest evolutionary stages?

In an effort to study a larger source sample with respect to its chemical evolution, we observed 21 massive star-forming regions covering all evolutionary stages from IRDCs via HMPOs/hot cores to UCHII with the APEX telescope at submm wavelengths (Beuther et al. subm.). While most spectral lines were detected mainly toward the HMPO/hot core sources, the ethynyl molecule C_2H is omni-present toward all regions. To get an idea about the spatial structure of ethynyl, we went back to an older SMA data-set targeting the HMPO IRAS 18089-1732 at the same frequency around 349.4 GHz of the C_2H line (Beuther et al. 2005c). Because we were not able to image the spatial distribution of C_2H at that time, we now restricted the data to only the compact configuration allowing us to better image the larger-scale distribution of the gas. Figure 10 presents the resulting molecular line map, and we find that C_2H is distributed in a shell-like fashion around the central protostellar condensation. Comparing this with all other imaged molecules in the original paper, only C_2H exhibits this behavior. To better understand this effect, we ran a set of chemical models in 1D for a cloud of 1200 $M_\odot$, a density power-law

$\rho \propto r^{-1.5}$ and different temperature distributions $T \propto r^q$. A snapshot of these models after an evolutionary time of 5×10^4 yrs is presented in Figure 10. The models reproduce well the central C_2H gap in IRAS 18089-1732 which should have approximately the same age.

Figure 10: The left panel presents in grey-scale the C_2H emission and in thick solid contours the corresponding submm continuum from the SMA toward the HMPO IRAS 18089-1732 (Beuther et al., subm.). The right panel shows a chemical model explaining the decreased emission toward the core center after approximately 5×10^4 yrs. The parameter q denotes the temperature power-law index, and the T values refer to the temperature at the core edge or to isothermal values ($q = 0$).

While these models reproduce the observations, they give also predictions how the C_2H emission should look like at different evolutionary times. In particular, C_2H forms quickly early on, also at the core center. Since not many molecules exist which do not freeze out and are available to investigate the cold early phases of massive star formation (valuable exceptions are, e.g., NH_3 or N_2H^+), the detection of C_2H toward the whole sample in combination with the chemical models triggers the prediction that C_2H may well be an excellent molecule to investigate the physical conditions of (massive) star-forming regions at very early evolutionary stages. High-spatial-resolution observations of IRDCs are necessary to investigate this potentially powerful astrophysical tool in more detail.

5.3 Employing molecules as astrophysical tools

While the chemical evolution of massive star-forming regions is interesting in itself, one also wants to use the different characteristics of molecular lines to trace various physical processes. In contrast to molecules like SiO and CO that are well-known outflow/jet tracers, the task gets more difficult searching for suitable accretion disk tracers. Investigating our sample and disk claims in the literature, one finds that in many cases exclusively one or the other molecule allows the investigation of rotational motion, whereas most other molecular lines remain without clear signatures. For example, the $HN^{13}C$ line discussed above (§5.1) traces rotation in the hot core G29.96 but it is not even detectable in younger sources. The other way around, $C^{34}S$ traced disk rotation in the young HMPO IRAS 20126 (Cesaroni et al. 2005), but not anymore toward more evolved sources (§5.1). These differences imply that one will unlikely find a uniquely well suited molecular line allowing the study of large samples of massive accretion disks, but that one has to select for each source or source class the suitable molecule for detailed investigations.

In the following, I give a short table with molecules and their potential usefulness to study different physical processes. This table (1) is restricted to molecules with spectral lines at cm/(sub)mm wavelengths and does not claim any kind of completeness, it should just serve as a rough overview and it only lists the main isotopologues of each species.

OH	Zeeman effect, magnetic fields, maser signpost of star formation
CO	General cloud structure, outflows
SiO	Shocks due to jets/outflows
CO^+	Far-UV radiation from embedded protostars
CS	Dense gas, rotation, also outflows
CN	Photodominated regions, Zeeman effect, magnetic fields
SO	Shocks, dense gas
H_2O	Shocks and hot cores, rotation ($H_2^{18}O$), maser signpost of star formation
HDO	Deuterium chemistry
H_2D^+	Cold gas, pre-stellar cores, freeze out
HCN	Dense cores, also outflows
HNC	Dense cores, rotation ($HN^{13}C$)
HCO^+	Outflows, infall, cosmic rays, ionization degree, dense gas ($H^{13}CO^+$)
SO_2	Shocks, dense gas
C_2H	Early evolutionary stages (§5.2)
N_2H^+	Early evolutionary stages
N_2D^+	Deuteration, freeze out
H_3O^+	Cosmic rays
H_2CO	Dense gas, temperatures
NH_3	Cold and hot cores, rotation, temperatures
CH_3OH	Shocks, young rotating structures? (§3.1), temperatures, maser signpost of massive star formation
CH_3CN	Hot cores, temperatures, rotation
CH_3CCH	Dense gas, temperatures
$HCOOCH_3$	Hot cores, rotation
CH_3CH_3CN	Hot Cores

Table 1: A few useful molecules and some of their potential applications.

6 Conclusions and summary

This article tries to outline how far we can currently constrain physical and chemical properties in massive star formation using (sub)mm interferometry. Coming back to the original questions raised in the abstract: (a) What are the physical conditions at the onset of massive star formation? (b) What are the characteristics of potential massive accretion disks and what do they tell us about massive star formation in general? (c) How do massive clumps fragment, and what does it imply to high-mass star formation? (d) What do we learn from imaging spectral line surveys with respect to the chemistry itself as well as for utilizing molecules as tools for astrophysical investigations?

Can we reasonably answer any of these questions with confidence? There are no clear-cut answers possible yet, however, the observations are paving a

way to shedding light on many of the issues, and one can try to give tentative early answers. The following is a rough attempt to outline the directions for current and future answers in these fields:

(a) Massive gas clumps prior or at the onset of high-mass star formation are characterized by cold temperatures of the order 15 K and small line-widths indicative of a low level of turbulence. Their molecular abundances appear comparable to those of low-mass starless cores. Interestingly, the outflow detection rates toward IRDCs are high, and no genuine High-Mass Starless Cores have been reported in the literature yet. Although the statistical basis is not solid enough yet, this allows us to speculate that the high-mass starless phase is likely to be very shortlived.

(b) The detection of a real accretion disk around a massive protostar still remains an open issue. However, we find many rotating structures in the vicinity of young massive star-forming regions all the way from IRDCs to Hot Molecular Cores. These structures are on average large with sizes between 1×10^3 and 2×10^4 AU, and they have masses of the order of the central protostar. Hence, most of them are not Keplerian accretion disks but rather some larger-scale rotating/infalling structures or toroids that may feed more genuine accretion disks in the so far unresolved centers of these regions.

(c) Fragmentation of massive star-forming regions is frequently observed, and the core mass function of one young region is consistent with the Initial Mass Function. However, caveats of unknown temperature distributions or missing flux on larger scales may still affect the results. Furthermore, we find proto-trapezium like structures which show multiple bound sources on small scales of a few 1000 AU implying protostellar densities of the order 10^5 protostars/pc^{-3}. Such densities are still not sufficient to allow coalescence, however, it may be possible to find even higher protostellar densities with the improved observational capabilities of future instruments. Although mergers do not appear necessary to form massive stars in general, they still remain a possibility for the most massive objects.

(d) Astro-chemistry is a young branch in astrophysical research, and we are currently only touching the surface of its potential. The different paths to follow in the coming years are manyfold: With larger source-samples, we will be able to derive a real chemical evolutionary sequence with one of the goals to use chemistry as an astrophysical clock. Furthermore, understanding the chemical differences is important to use the molecular lines as astrophysical tools to investigate the physical processes taking place. Moreover, another current hot topic is planet formation, and in this context astro-biology is a rising subject. In this regard understanding astro-chemistry and detecting new and more complex molecules in space is paving the way for future astro-biological science.

Acknowledgments: Thanks a lot to Cassie Fallscheer and Javier Rodon for preparing the figures related to the IRDC 18223-3 outflow/disk system and the W3-IRS5 fragmenting core. I further acknowledge financial support by the Emmy-Noether-Program of the Deutsche Forschungsgemeinschaft (DFG, grant BE2578).

References

Andre, P., Ward-Thompson, D., & Barsony, M. 2000, Protostars and Planets IV, 59

Arce, H. G., Shepherd, D., Gueth, F., et al. 2007, in Protostars and Planets V, ed. B. Reipurth, D. Jewitt, & K. Keil, 245–260

Bachiller, R., Pérez Gutiérrez, M., Kumar, M. S. N., & Tafalla, M. 2001, A&A, 372, 899

Bally, J. & Zinnecker, H. 2005, AJ, 129, 2281

Beuther, H., Churchwell, E. B., McKee, C. F., & Tan, J. C. 2007a, in Protostars and Planets V, ed. B. Reipurth, D. Jewitt, & K. Keil, 165–180

Beuther, H., Hunter, T. R., Zhang, Q., et al. 2004a, ApJ, 616, L23

Beuther, H., Leurini, S., Schilke, P., et al. 2007b, A&A, 466, 1065

Beuther, H. & Schilke, P. 2004, Science, 303, 1167

Beuther, H., Schilke, P., & Gueth, F. 2004b, ApJ, 608, 330

Beuther, H., Schilke, P., Menten, K. M., et al. 2002a, ApJ, 566, 945

Beuther, H., Schilke, P., Sridharan, T. K., et al. 2002b, A&A, 383, 892

Beuther, H. & Shepherd, D. 2005, 105

Beuther, H. & Sridharan, T. K. 2007, ApJ, 668, 348

Beuther, H., Sridharan, T. K., & Saito, M. 2005a, ApJ, 634, L185

Beuther, H. & Steinacker, J. 2007, ApJ, 656, L85

Beuther, H. & Walsh, A. 2008, ApJ in press, arXiv:0712.0579

Beuther, H., Zhang, Q., Bergin, E. A., et al. 2007c, A&A, 468, 1045

Beuther, H., Zhang, Q., Greenhill, L. J., et al. 2005b, ApJ, 632, 355

Beuther, H., Zhang, Q., Hunter, T. R., Sridharan, T. K., & Bergin, E. A. 2007d, A&A, 473, 493

Beuther, H., Zhang, Q., Hunter, T. R., et al. 2004c, ApJ, 616, L19

Beuther, H., Zhang, Q., Sridharan, T. K., & Chen, Y. 2005c, ApJ, 628, 800

Blake, G. A., Mundy, L. G., Carlstrom, J. E., et al. 1996, ApJ, 472, L49

Blake, G. A., Sutton, E. C., Masson, C. R., & Phillips, T. G. 1987, ApJ, 315, 621

Bonnell, I. A., Larson, R. B., & Zinnecker, H. 2007, in Protostars and Planets V, ed. B. Reipurth, D. Jewitt, & K. Keil, 149–164

Bonnell, I. A., Vine, S. G., & Bate, M. R. 2004, MNRAS, 349, 735

Cabrit, S. & Bertout, C. 1990, ApJ, 348, 530

Carey, S. J., Feldman, P. A., Redman, R. O., et al. 2000, ApJ, 543, L157

Cesaroni, R., Churchwell, E., Hofner, P., Walmsley, C. M., & Kurtz, S. 1994, A&A, 288, 903

Cesaroni, R., Galli, D., Lodato, G., Walmsley, C. M., & Zhang, Q. 2007, in Protostars and Planets V, ed. B. Reipurth, D. Jewitt, & K. Keil, 197–212

Cesaroni, R., Hofner, P., Walmsley, C. M., & Churchwell, E. 1998, A&A, 331, 709

Cesaroni, R., Neri, R., Olmi, L., et al. 2005, A&A, 434, 1039

Egan, M. P., Shipman, R. F., Price, S. D., et al. 1998, ApJ, 494, L199

Gueth, F., Bachiller, R., & Tafalla, M. 2003, A&A, 401, L5

Hatchell, J. & van der Tak, F. F. S. 2003, A&A, 409, 589

Keto, E. 2007, ApJ, 666, 976
Krumholz, M. R., Klein, R. I., & McKee, C. F. 2007a, ApJ, 665, 478
—. 2007b, ApJ, 656, 959
Lada, C. J. & Lada, E. A. 2003, ARA&A, 41, 57
Launhardt, R. 2004, in IAU Symposium, 213
Leurini, S., Beuther, H., Schilke, P., et al. 2007, A&A, 475, 925
McKee, C. F. & Ostriker, E. C. 2007, ARA&A, 45, 565
McKee, C. F. & Tan, J. C. 2002, Nature, 416, 59
—. 2003, ApJ, 585, 850
Megeath, S. T., Wilson, T. L., & Corbin, M. R. 2005, ApJ, 622, L141
Motte, F., Andre, P., & Neri, R. 1998, A&A, 336, 150
Motte, F., Bontemps, S., Schilke, P., et al. 2007, ArXiv e-prints, 0708.2774, 708
Mueller, K. E., Shirley, Y. L., Evans, N. J., & Jacobson, H. R. 2002, ApJS, 143, 469
Nomura, H. & Millar, T. J. 2004, A&A, 414, 409
Noriega-Crespo, A., Morris, P., Marleau, F. R., et al. 2004, ApJS, 154, 352
Padoan, P. & Nordlund, Å. 2002, ApJ, 576, 870
Parker, N. D., Padman, R., & Scott, P. F. 1991, MNRAS, 252, 442
Piétu, V., Dutrey, A., & Guilloteau, S. 2007, A&A, 467, 163
Pillai, T., Wyrowski, F., Carey, S. J., & Menten, K. M. 2006a, A&A, 450, 569
Pillai, T., Wyrowski, F., Menten, K. M., & Krügel, E. 2006b, A&A, 447, 929
Rathborne, J. M., Jackson, J. M., Chambers, E. T., et al. 2005, ApJ, 630, L181
Rathborne, J. M., Jackson, J. M., & Simon, R. 2006, ApJ, 641, 389
Reynolds, S. P. 1986, ApJ, 304, 713
Ridge, N. A. & Moore, T. J. T. 2001, A&A, 378, 495
Salpeter, E. E. 1955, ApJ, 121, 161
Schilke, P., Groesbeck, T. D., Blake, G. A., & Phillips, T. G. 1997, ApJS, 108, 301
Shepherd, D. S. & Churchwell, E. 1996, ApJ, 457, 267
Simon, M., Dutrey, A., & Guilloteau, S. 2000, ApJ, 545, 1034
Simon, R., Jackson, J. M., Rathborne, J. M., & Chambers, E. T. 2006, ApJ, 639, 227
Sridharan, T. K., Beuther, H., Saito, M., Wyrowski, F., & Schilke, P. 2005, ApJ, 634, L57
Sridharan, T. K., Beuther, H., Schilke, P., Menten, K. M., & Wyrowski, F. 2002, ApJ, 566, 931
Tafalla, M., Santiago-García, J., Myers, P. C., et al. 2006, A&A, 455, 577
van der Tak, F. F. S., Tuthill, P. G., & Danchi, W. C. 2005, A&A, 431, 993
Ward-Thompson, D., Motte, F., & Andre, P. 1999, MNRAS, 305, 143
Yorke, H. W. & Sonnhalter, C. 2002, ApJ, 569, 846
Zhang, Q., Hunter, T. R., Brand, J., et al. 2005, ApJ, 625, 864
Zinnecker, H. & Yorke, H. W. 2007, ARA&A, 45, 481

This figure "05358_uv.jpg" is available in "jpg" format from:

http://arXiv.org/ps/0712.1109v1


This figure "18089_cch_bw.jpg" is available in "jpg" format from:
http://arXiv.org/ps/0712.1109v1

This figure "18089_int_mom.jpg" is available in "jpg" format from:

http://arXiv.org/ps/0712.1109v1


This figure "ch3oh_mom1c_bw.jpg" is available in "jpg" format from:
http://arXiv.org/ps/0712.1109v1

This figure "f1.jpg" is available in "jpg" format from:

http://arXiv.org/ps/0712.1109v1

This figure "mdc1.jpg" is available in "jpg" format from:

http://arXiv.org/ps/0712.1109v1

This figure "f2.jpg" is available in "jpg" format from:

http://arXiv.org/ps/0712.1109v1

This figure "g29.jpg" is available in "jpg" format from:

http://arXiv.org/ps/0712.1109v1

This figure "C2H_t50000.ilm_rotate.jpg" is available in "jpg" format from:

http://arXiv.org/ps/0712.1109v1

This figure "sed_mm3_biermann_v2.jpg" is available in "jpg" format from:

http://arXiv.org/ps/0712.1109v1

This figure "w3irs5.jpg" is available in "jpg" format from:

http://arXiv.org/ps/0712.1109v1